Progress in
PHOTOVOLTAICS

PROGRESS IN PHOTOVOLTAICS: RESEARCH AND APPLICATIONS
*Prog. Photovolt: Res. Appl.* 2013; **21**:933–941
Published online 27 March 2012 in Wiley Online Library (wileyonlinelibrary.com). DOI: 10.1002/pip.2180

RESEARCH ARTICLE

# Calculation of quantitative shunt values using photoluminescence imaging

Yael Augarten[1]*, Thorsten Trupke[1], Martha Lenio[1], Jan Bauer[2], Juergen W. Weber[3], Matthias Juhl[1], Martin Kasemann[4] and Otwin Breitenstein[2]

[1] University of New South Wales, ARC Photovoltaics Centre of Excellence, Sydney, New South Wales, Australia
[2] Max Planck Institute of Microstructure Physics, Exp. Dep II, Halle, Germany
[3] BT Imaging, Sydney, New South Wales, Australia
[4] University of Freiburg, Freiburg, Germany

## ABSTRACT

A proof of concept study for a method of determining quantitative shunt values in silicon solar cells from photoluminescence images is presented. The method is based on interpretation of the luminescence intensity around a local shunt or recombination-active defect in terms of the extracted current. The theoretical relationship between the photoluminescence signal and the shunt current is derived. Experimental results on specifically prepared test structures show good agreement with known shunt resistance values. Experimental data on diffused wafers are presented. The effect of the front metallisation in complete cells on the appearance and interpretation of shunts in photoluminescence images is investigated experimentally. The limitations of the method are discussed. Copyright © 2012 John Wiley & Sons, Ltd.

**KEYWORDS**

silicon solar cells; photoluminescence imaging; shunts; shunt current

***Correspondence**

Yael Augarten, University of New South Wales, ARC Photovoltaics Centre of Excellence Sydney, New South Wales, Australia.
E-mail: y.augarten@student.unsw.edu.au

Received 28 February 2010; Revised 31 January 2010; Accepted 25 January 2012

## 1. INTRODUCTION

Shunting commonly refers to local internal short circuits in a solar cell. More generally, shunts are described in the common equivalent circuit of a solar cell as a low esistance path that is parallel to the junction. Shunts can reduce the cell efficiency and can cause hot spot heating in modules. Severe shunts therefore reduce the solar cell manufacturing yield. Existing methods of shunt detection can be classified into one of two categories: spatially resolved and non-spatially resolved methods. Non-spatially resolved methods, such as reverse bias current measurements or the analysis of *I–V* curves, can be fast (on the order of milliseconds) but provide only global information on cell properties. Mapping and imaging methods, on the other hand, can provide spatially resolved information but usually have measurement times on the order of several seconds to hours and are often contacted. Current spatially resolved shunt detection methods are solar cell local characterisation [1] for localising shunts, Corescan [2], electron/light beam-induced current measurements [3,4], illuminated and dark lock-in thermography [5], spatially resolved hot-spot detection under high reverse bias [6], photoluminescence (PL) and electroluminescence imaging [7,8], and liquid crystal sheet methods [9,10].

With a typical imaging time on the order of 1 s for 156 mm wafers and cells, PL and electroluminescence imaging have the potential to be useful inline characterisation tools [7,8]. Currently, PL images can be used to quantitatively determine several spatially resolved cell parameters, including minority carrier lifetime [8], series resistance [11,12], saturation current density [13], and front and rear surface recombination [14]. Shunt detection by luminescence imaging has also been demonstrated; however, previous work on this topic has been largely qualitative [15,16].

This paper presents a proof of concept for a method of obtaining quantitative values for the total recombination current in local shunts or defects from open circuit PL images. The method can be applied to both diffused wafers and fully processed solar cells. The theory behind the method and its limitations are discussed. Experimental results for verification of the theory and application of the method to shunted diffused wafers are presented. With the method presented here, a single PL image is analysed, and as such, it is not

Copyright © 2012 John Wiley & Sons, Ltd.

able to distinguish between linear shunts and non-linear local recombination sites. It is therefore equally applicable to calculate the current losses for both types of defects. In this paper, the term 'shunts' refers to both types of defects.

## 2. THEORY

Photoluminescence imaging measures the spatially resolved radiative band-to-band recombination of an illuminated sample. The PL signal of a silicon sample is given as [17–19]

$$PL = C \cdot \exp\left( {}^{V_d}/_{V_t} \right) \quad (1)$$

where $C$ is a calibration constant depending on the optical properties, geometry and carrier lifetime of the sample, $V_d$ is the diode (junction) voltage, and $V_t$ is the thermal voltage (25.8 mV at 25 °C). The contribution of diffusion limited carriers to the PL signal can be considered negligible at open circuit [12,20] and was not included in Equation 1. The local shunt resistance $R_{sh}$ at a given voltage is obtained from

$$R_{sh} = \frac{V_{R_{sh}}}{I_{R_{sh}}} \quad (2)$$

where $V_{R_{sh}}$ is the local voltage at the shunt and $I_{R_{sh}}$ is the total current flowing into the shunt.

Both of these parameters can be calculated from an open circuit PL image.

To calculate a local voltage from a PL image, the proportionality constant $C$ is first calculated from Equation 1, relating the intensity of the open circuit PL image averaged over the entire cell area with the measured open circuit voltage $V_{oc}$. Once $C$ is determined, the voltage at the shunt $V_{R_{sh}}$ can then be calculated from Equation 1 with the $PL$ term given as the lowest PL signal in the shunted region, because that ciresponds to the location of the shunt. This calculation assumes that $C$ is constant across the entire cell area, which is not necessarily true because the lifetime and optical properties of different cell regions can vary. However, because of the exponential relationship between PL intensity and diode voltage (Equation 1), small lateral variations in the calibration constant will contribute only small relative errors to the shunt voltage and hence to the measured shunt resistance.

### 2.1. Calculation of the shunt current

A local shunt in an illuminated solar cell represents a local current sink. The shunt itself is often only a few micrometres in diameter [21], that is, much smaller than the area represented by a single pixel (165 μm in the PL imaging system that was used in this work) and, thus, not visible in large area luminescence images. A local shunt extracts current from the surrounding non-shunted area through the emitter, reducing the voltage and hence the PL signal of the non-shunted area. The shunt thus appears in a PL image as a circular or elliptical blurred region of reduced luminescence intensity, as has been described previously [16,22]. That is, the blurred circular regions seen in PL images show the *effect* of a shunt (or local recombination-active defect) on the surrounding non-shunted (defect free) cell region rather than the shunt itself (Figure 1). This is a similar effect to lock-in thermography images, in which heat is generated at the location of the shunt, but it is the propagation of that heat into the surrounding cell area that is visible in the images [5]. The shunt current $I_{R_{sh}}$ is the total current flowing into the shunt from the surrounding cell region. It should be noted that the PL method is not applicable on a microscopic scale, because like lock-in thermography, the method is based on analysing the impact a local shunt has on the PL signal in its surrounding. $I_{R_{sh}}$ can be calculated from an open circuit PL image as follows.

The dark diode current density $J_{d,i}$ of each area $i$ within a solar cell can be described by the Shockley diode equation

$$J_{d,i} = J_{01,i} \cdot \exp\left( {}^{V_{d,i}}/_{n_i} V_t \right) \quad (3)$$

with $V_{d,i}$, $n_i$, and $J_{01,i}$ the local diode voltage, ideality factor, and dark saturation current density of the area $A_i$.

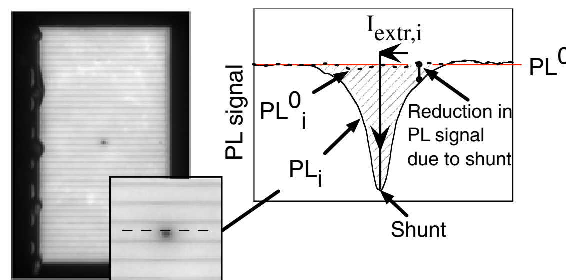


**Figure 1.** Left: photoluminescence (PL) image of a laboratory solar cell with a single point-like shunt. Right: cross section of the PL signal across the shunt (black curve). The straight red line gives the global non-shunted PL signal $PL^0$. $I_{Rsh}$ is proportional to the difference in the PL signal between the two regions (shaded area).


*Prog. Photovolt: Res. Appl.* 2013; **21**:933–941 © 2012 John Wiley & Sons, Ltd.
DOI: 10.1002/pip

Combining Equation 1 with the Shockley diode equation gives

$$J_{d,i} = \frac{J_{01,i}}{C_i^{1/n}} \cdot (PL_i)^{1/n} \tag{4}$$

In each cell element $i$, the locally extracted current density $J_{extr,i}(V_{d,i})$ is given as

$$J_{extr,i}(V_{d,i}) = J_L - J_{d,i}(V_{d,i}) \tag{5}$$

with $J_L$ the light generated current density, which is assumed to be uniform across the cell area, i.e. independent of $i$. Combining Equations (4) and (5) and assuming $n = 1$ gives

$$PL_i = \frac{C_i}{J_{01,i}} (J_{L,i} - J_{extr,i}) \tag{6}$$

The local PL signal thus decreases in proportion to the extracted current density. From an area with zero current extraction, we have

$$PL_i^0 = \frac{C_i}{J_{01,i}} \cdot J_{L,i} \tag{7}$$

$PL_i^0$ is thus the PL signal that would be expected from the area $i$ in the absence of the nearby shunt or local defect. Combining Equations 6 and 7 gives

$$J_{extr,i} = J_L \cdot \left(1 - \frac{PL_i}{PL_i^0}\right) \tag{8}$$

The current extracted from pixel $i$ is then obtained by multiplying $J_{extr,\,i}$ by the area represented by a pixel $A_i$:

$$I_{extr,i} = J_L \cdot \left(1 - \frac{PL_i}{PL_i^0}\right) \cdot A \tag{9}$$

In Equation 9, the local parameters $C_i$ and $J_{01,i}$ cancel out in the PL intensity ratio. The total current extracted by a local shunt, $I_{R_{sh}}$, is obtained by summing the locally extracted current acciding to Equation 9 over all pixels that are affected by the shunt. That summation can be performed in two different ways, which we will refer to as the *local* $PL^0$ *method* and the *global* $PL^0$ *method*, respectively.

#### 2.1.1. Local $PL^0$ method

In this method, the local PL signal with zero current extraction $(PL_i^0)$ must be known for each pixel within the area that is affected by the shunt. The method requires a PL image of the sample with and without shunting, that is, before and after the shunt has been introduced. $PL_i^0$ is the PL signal from each pixel in the non-shunted image. This method can be applied in situations where localised shunts or defects are introduced into a wafer or solar cell without significantly impacting the cell or material properties outside the local defect, for example, shunting introduced during laser doping or selective emitter formation or during low temperature processes such as metal plating. In cases where sister wafers are processed, $PL_i^0$ may be taken from a PL image of the unaffected sister wafer.

The area to be analysed (i.e. the area affected by the shunt) is selected from the shunted image, and the shunt current is given by

$$I_{R_{sh},PL} = \sum_i J_L \cdot \left(1 - \frac{PL_i}{PL_i^0}\right) \cdot A_i \tag{10}$$

The shunt current is thus given as the sum of all pixels in the area that is affected by the shunt. In practice, this summation is achieved conveniently using image analysis programs. This approach is similar to the thermography method proposed by Breitenstein *et al.*, which relies on averaging the thermal signal over an area large enough to capture the total heat dissipated in a shunt [23]. The local $PL^0$ method will be experimentally demonstrated below using test structures with artificially introduced shunts.

#### 2.1.2. Global $PL^0$ method

In many practical cases, a local shunt or defect can be observed in a PL image, but the corresponding local information $PL_i^0$ is not available, for example, shunts introduced during the crystallisation, for example, because of SiC filaments [19], emitter diffusion steps, or edge isolation of the solar cell. In these cases, a global value $PL^0$ is used in Equation 10 instead of the local $PL_i^0$. The global value can be obtained either from a homogeneous non-shunted area of the sample or from the PL signal at the circumference of the defect affected area in the PL image as shown in Figure 1. The implicit assumption of constant $C_i$ and $J_{01,i}$ is made in that case, which is well justified for monocrystalline samples and for shunts located in single grains of multicrystalline samples. The case of shunts located in regions with non-uniform lifetime is discussed in the limitations section.

The local $PL^0$ method is more accurate and therefore preferable in scenarios where the local PL intensity prior to shunting is available. The errors associated with using the global $PL^0$ method will be discussed in the experimental section.

## 3. EXPERIMENTAL

In the following experiments, $I_{R_{sh},PL}$ is calculated for local shunts from PL images of diffused wafers, using Equation 10. The assumption of $n = 1$ is investigated, for the cases of current extraction from an entire cell and from a local defect.

### 3.1. Relationship between photoluminescence signal and $I_{extr}$

This experiment was performed on industrial 6-in multicrystalline silicon solar cells, with the aim of experimentally verifying the proportionality between the PL ignal and the extracted current density expressed in Equation 6. PL images of several cells were taken with constant illumination and at various operating points between $I_{sc}$ and $V_{oc}$. As an example, Figure 2 shows the average PL intensity of the entire cell as a function of the extracted current ($I_{extr}$) for one specific cell. The dashed line is a linear fit to the data, for $I_{extr} < 0.971_{sc}$.

All cells used in this work showed similar linear relationships, although with varying gradients (because of differing $I_{01}$) and $y$-intercepts ($PL^0_{V_{oc}}$). Thus, for all investigated cells, the cell averaged PL signal was found to be linearly proportional to the total current extracted from the cell for $I_{extr} < 0.971_{sc}$ (approximately $V_{mp} < V_{cell}$ $V_{oc}$), meaning that the assumption of $n = 1$ was valid in this range. Figure 2 also shows that the average PL count converges towards a constant value for currents exceeding the short circuit current. That signal is caused by diffusion-limited carriers as discussed elsewhere [12]. For greater accuracy in the analysis of PL images at $V < V_{mp}$, this signal is subtracted from the measured signal.

### 3.2. Ideal shunt case

Shunting results in extended regions within the $I$–$V$ curve with high ideality factor ($n > 1$), particularly at low voltages. It could therefore be argued that $n = 1$ is not a valid assumption in a shunt analysis method, and the above analysis is therefore not valid. However, in the case of localised shunts or defects, the majority of the affected region that is analysed in a PL image is not shunted and is operating at voltages $V > V_{mpp}$, where $n = 1$ is valid. The following experiment was performed to measure the effect of a *local* current extraction on the PL signal and to obtain quantitative values of the local shunt current.

A solar cell structure was fabricated with an inkjet-printed buried-contact scheme on a monocrystalline wafer. The structure had a full rear metallisation, approximately 100 Ω/□ front side emitter diffusion, but only a single metallised square contact (side length 500 μm) on the front surface. A variable artificial local shunt was created by externally connecting a resistor of known value in parallel with the cell, that is, between the full area rear metallization and the front point contact, using a fine probe to contact the front contact pad. The voltage across the external resistor was measured under illumination, and the current extracted through the resistor, $I_{R_{known}}$, was calculated using Ohm's law.

Photoluminescence images were taken on that test structure with various illumination intensities for 12 external resistor values between 1 and 400 Ω plus one image taken with an open circuit. Figure 3 shows three PL images taken from the test structure with identical illumination intensity but with different external resistor values. They show the expected blurred circular regions, which increase in radius and severity as the shunt resistance is decreased. The local $PL^0$ method as described above was applied to those images; that is, $I_{R_{sh},PL}$ was calculated from Equation 10. To avoid error introduced by the contact probe, we selected only the top half of the shunt-affected area for analysis, and the calculated $I_{R_{sh},PL}$ was then multiplied by two. The comparison between the measured current and the current obtained from the PL image as described above is shown in Figure 4.

Good agreement is observed between the current values obtained from the PL image and from the measured currents. A linear fit to the data had a gradient of 1.06, close to the theoretically expected gradient of 1. This corresponds to a standard deviation of approximately 5% and, thus, an error in $I_{R_{sh},PL}$ of approximately 10%. The majority of this error is due to statistical error in the PL signals of the shunted and non-shunted images. Less than 1% of this error is caused by the combined effects of the contact patch and the uncertainty in the measurement of $V_{R_{known}}$.

For comparison $I_{R_{sh},PL}$ was also calculated using the global $PL^0$ method from the same PL images but with the global $PL^0$ value taken as the average PL count rate at the circumference of the shunted region, as shown on

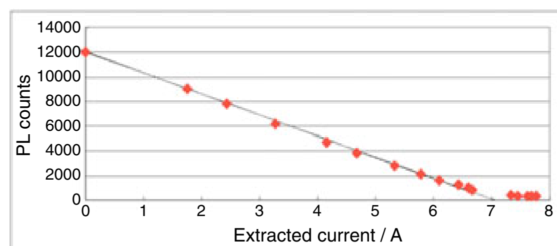


**Figure 2.** The photoluminescence (PL) signal from an industrial multicrystalline silicon solar cell as a function of the current extracted from the cell. Measurements were taken at constant illumination intensity but at different operating points between short circuit and open circuit. The dashed line is a linear fit to the data for $I_{extr} < 0.971_{sc}$. The constant offset in the PL signal that is observed at extracted currents exceeding 7 A is due to diffusion-limited carriers [20]. The PL signals in this graph are not corrected for this effect.


*Prog. Photovolt: Res. Appl.* 2013; **21**:933–941 © 2012 John Wiley & Sons, Ltd.
DOI: 10.1002/pip

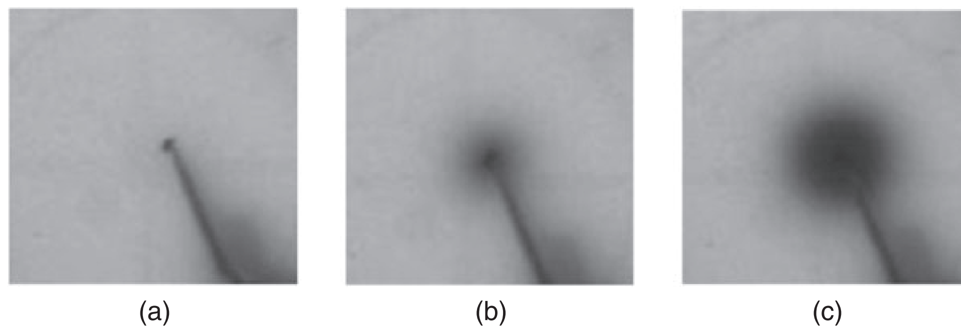


**Figure 3.** Photoluminescence image of an experimental test structure (see text) at open circuit, that is, (a) with no external shunt resistance, (b) with a 120-Ω shunt resistance and (c) with 22-Ω shunt resistance. All images are shown on the same relative colour scale.

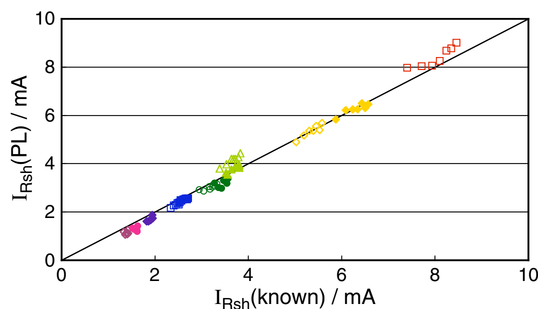


**Figure 4.** Comparison of shunt current values calculated from photoluminescence images (*y*-axis) with the measured values, for 12 resistor values ranging from 1 to 400 Ω. Values were calculated for seven illumination intensities between 0.24 and 1 sun for each resistor. Each symbol shows the results for each resistor, and the solid line represents $y = x$.

the right-hand side of Figure 1. Practically, this was achieved by taking the average PL signal over a semicircle several pixels wide at the edge of the analysed area. In this case, a similar linear relationship between $I_{R_{sh},PL}$ and $I_{R_{known}}$ is observed, but with a gradient of 1.12. For monocrystalline samples, which exhibit little variation in effective lifetime, of shunts within a single grain on a multicrystalline wafer, the global $PL^0$ method thus provides a convenient means to obtain quantitative information about shunt or recombination currents flowing into local shunts or defects. If this method of estimating $PL^0$ is used, then a similar accuracy is expected for shunts located across two or more different lifetime grains; however, this accuracy has not been experimentally tested.

From these experiments, it was concluded that the proportionality in Equation 6 holds and that the assumption of $n = 1$ is valid in the vicinity of a local shunted area. This method could be used to quantitatively analyse the current lost to active shunts or local recombination sites in wafers at any point prior to the front metallisation. The key in each of these cases is the ability to obtain (i.e. measure or estimate) the PL signal that would be measured in the defect-affected area in the absence of the defect.

Multicrystalline silicon contains a large number of local defects, which occur as line-shaped features, such as dislocation networks and recombination-active grain boundaries. Previously, the reduction in PL intensity in the vicinity of such local defects has been interpreted as a local change in the depth-dependent carrier profile caused by a reduced bulk diffusion length [7]. Although this interpretation is valid for extended bulk regions with reduced diffusion length, it is not expected to be valid around local microscopic defects [24]. For local defects, the interpretation in terms of a lateral current extraction from surrounding non-defected regions, as described by the above analysis, is more appropriate. This interpretation allows the global $PL^0$ method to be applied to such features. The global $PL^0$ signal could be obtained by extrapolation of PL intensity of a cross section of the defect, as shown in Figure 1, and the recombination current per unit length could be obtained for these line-shaped local defects for example.

Single PL images as shown in Figure 5 do not allow distinguishing whether the reduction in PL signal is caused by an extended defect with a circular shape or by a point-like defect, which extracts current via the emitter. The methodology described here correctly describes both situations; in the former case, it results in the total additional recombination current caused by the extended defect, in the latter case the total current extracted by the local defect. We would also like to note that circuit modelling shows that the linear or non-linear nature of a defect can be determined from the analysis of PL images taken with different illumination intensities using the methodology described here.

### 3.3. Application to finished cells

A known source of error when attempting to quantify shunts from PL images is the effect of current extraction through the front metal grid, which has been modelled by Kasemann *et al.* [22,25]. If a shunt is located near a front grid finger, the low resistance of the metal allows current

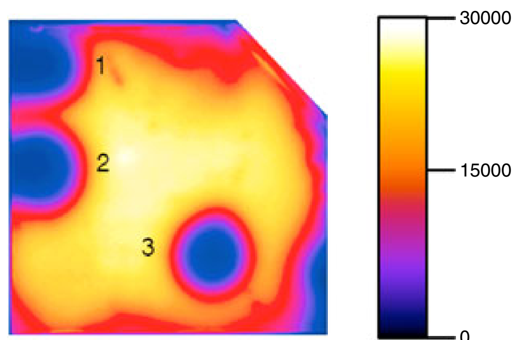


**Figure 5.** A photoluminescence (PL) image of a float zone wafer contaminated during emitter diffusion taken at 1-sun equivalent illumination. The wafer shows three blurred circular regions indicating point-like defects or shunts (numbered). The current extracted through these defects was calculated using the global $PL^0$ method with $PL^0$ equal to the average counts at the circumference of the shunted region as described above. The extracted current values are 26–30 mA in all three cases. The scale bar shows the PL signal in thousands of counts per second.

to be extracted from a significantly larger cell area, which decreases the effect of the shunt on the carrier density (and thus on the PL intensity) in the region immediately surrounding it. Because the metal grid is able to spread the impact of the shunt over large cell area, the measurable effect from the local PL signal becomes difficult to distinguish from other features in the PL image, except in the immediate surroundings of the shunt between metal fingers. This effect is relevant to all samples after front metallisation. Here, we demonstrate this effect experimentally and quantitatively measure its extent as a function of the emitter sheet resistance and of the distance from the nearest finger.

Four solar cells with an inkjet-printed buried-contact scheme and a full front grid metallisation with 2 mm finger spacing were fabricated. Additional square point contacts with a side length of 200 μm were placed between grid fingers located at variable distances of 200–1000 μm from the nearest finger (Figure 6). The samples had emitter sheet resistivities between 110 and 180 Ω/□ as measured by four-point probe. A range of artificial shunts (1–300 Ω) were introduced in parallel at the point contacts, as described above. PL images were taken on each test structure first with and without the external shunts at each of the point contacts. The local $PL^0$ method was then applied to each image.

Figure 6(a) shows the PL image of the test structure with an introduced shunt. The shunt is clearly visible, and the extent of the shunt in the direction perpendicular to the fingers appears to be restricted by the fingers, giving it an elliptical appearance. These images agree qualitatively with the modelling of Kasemann *et al*. [22]. The ratio image in Figure 6(b) was calculated by dividing a PL image of the shunted sample by the PL image without the shunt and shows the fraction of current extracted from each pixel. There are two points of interest in the ratio image. The first point is the current extraction through the fingers close to the shunt, which is not easily visible in a single PL image, and is marked by the solid rectangle in the ratio image. The second point, not directly relevant in the context of this work but still interesting, is the appearance of areas of current extraction in locations that appear unconnected to the shunt (arrows). The origin of these features is not unambiguously clarified at this stage but is thought to be because of regions of reduced contact resistance in the rear metal.

The ratio image in Figure 6(b) is an example of how the local $PL^0$ method can be used to quantitatively calculate the current flowing into a local defect because of local changes to the device: the counts per pixel in the ratio image represent the fraction $PL_i/PL_i^0$ from Equation 10. The total area affected by the shunt, including current extracted through the fingers, is given by the solid rectangle. The locally affected region, given by the dashed rectangle in Figure 6(b), is the area visibly affected by the shunt in the single PL image (Figure 6(a)) and does not include current extracted through the fingers.

Comparison of this 'local' shunt current with the total current flowing into the shunt gives $I_{frac}$, the fraction of the total shunt current extracted through the fingers, and hence the relative error. This calculation was carried out for all contact points on all samples, giving $I_{frac}$ as a function of both the distance of the shunt from the finger and the emitter sheet resistivities. The results are shown in Figure 7. Figure 7 (a) shows data for emitter sheet resistivities of 110 and 140 Ω/□ and Figure 7(b) for 160 and 180 Ω/□.

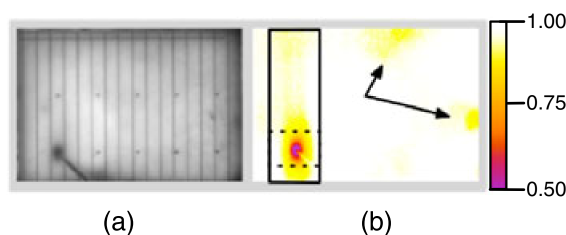


**Figure 6.** (a) A photoluminescence image of the test cell structure with a shunt introduced at the exact centre between two grid fingers. (b) The ratio image, which was calculated by dividing the shunted image by the non-shunted image (not shown). The ratio is equivalent to the fraction of current extracted from each pixel. Marked features are discussed in the text.


*Prog. Photovolt: Res. Appl.* 2013; **21**:933–941 © 2012 John Wiley & Sons, Ltd.
DOI: 10.1002/pip

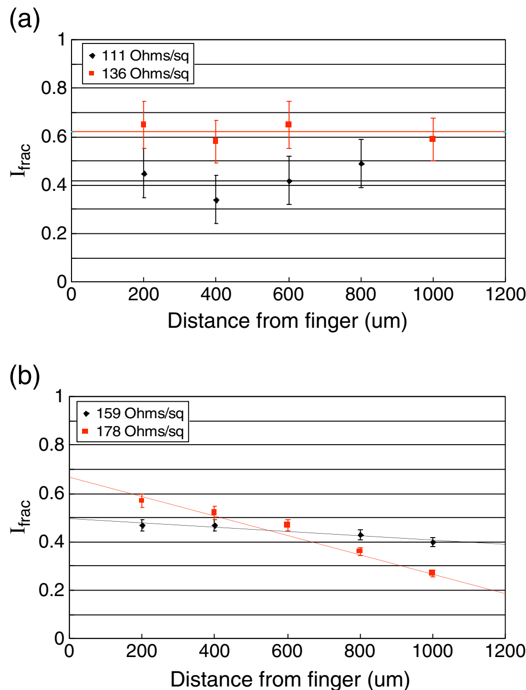


**Figure 7.** The fraction of shunt current extracted through the front metal grid fingers as a function of the distance of the shunt from the nearest finger, for emitter sheet resistivities of (a) 110 (diamonds) and 140 Ω/□ (squares) and (b) 160 (diamonds) and 180 Ω/□ (squares).

As the distance between the shunt and the nearest finger is increased, Figure 7(a) shows little variation in the fraction of current being supplied via the metal grid, while in Figure 7 (b), the fraction decreases as the distance of the shunt from the nearest finger increases.

These observations are qualitatively explained by the fact that increasing the distance to the nearest finger also decreases the distance to the opposite finger, affecting the amount of current extracted through that finger. For the lower sheet resistance values, as the distance from the nearest finger is increased, the decrease in the amount of current extracted is compensated or partially compensated by an increase in the current extracted by the opposite finger, resulting in very little change of $I_{frac}$ with distance. The higher sheet resistivities limit this effect, resulting in a decrease in $I_{frac}$ with increasing distance from the nearest finger.

This analysis of test structures shown above allows the impact of the metal grid on the appearance of the shunt to be quantified. In principle, look-up tables or analytic correction functions could be created to correct the calculated shunt current for the position of the shunt relative to the metal grid and the emitter sheet resistance. This would allow the shunt current for local shunts on complete solar cells to be calculated from a single PL image.

However, the fraction of current extracted through the fingers depends not only on the distance of the shunt from the metal grid and the emitter sheet resistance but also on other cell specific parameters, such as the contact resistance and the resistance of metal fingers. The inkjet-printed samples used in this proof of concept study showed unusually high variation in these parameters, making comparison of different contact points with individual samples and between samples, and hence the generation of a look-up table somewhat unreliable. The scatter in the data shown in Figure 7 is a result of these variations. Further work should focus on similar experiments on industrial solar cells, where contact resistance and finger resistance have less variability.

The data in Figure 7 show that the contribution of the current that is flowing in via the metal grid can be up to 70%, resulting in errors of up to a factor of 3 in the extracted current, if not accounted for. This effect is the main limitation of this method when applied to metallised cells in cases where the local $PL^0$ method is not feasible.

## 4. LIMITATIONS

The main assumption for the application of the local $PL^0$ method is that of an ideality factor $n = 1$. The experiments in this work and, more generally, experience from solar cell *I–V* curves measured in PV research and production show that this is a good approximation for both monocrystalline and multicrystalline solar cells at voltages above the maximum power point. Because the majority of the shunted sample area that is analysed in PL images with 1-sun illumination is at or above that voltage, there is very less experimental error associated with the local $PL^0$. Because the PL intensity ratio can be measured over the entire cell area and is not limited to the area between fingers immediately surrounding a shunt, the impact of a metal grid, while possibly large, is accounted for quantitatively in that method. Accurate shunt or defect recombination currents can be calculated as long as features in the ratio image can be unambiguously assigned to a specific defect. In cases where this is not possible, the total current value over the entire sample area is useful to assess the total additional recombination or shunt current caused by a specific process step.

For the analysis of a single PL image using the *global* $PL^0$ *method* (i.e. without PL data that are measured prior to introducing the defect being available), there are two main sources of error. In both wafers and cells, the choice of the global $PL^0$ value can significantly affect the calculated shunt current. However, $PL^0$ can be accurately determined from the PL signal in the circumference of local defects located in otherwise homogeneous material, such as in monocrystalline material or in large grains in multicrystalline samples, limiting the error to 5–10%. The second source of error is that of current extraction through the front metal grid in complete cells. As stated above, this can lead to very large deviations in the calculated current by up to 70%. The experiments in this study suggest that this error may be partially compensated on the basis of empirically determined lookup tables containing correction functions.

## 5. CONCLUSIONS

An approach for interpreting the reduction in PL signal around local defects (shunts and recombination active defects) in terms of the current extracted by the defect was presented. The theory for the method was derived, and limitations of the method were discussed. The method was demonstrated experimentally on specifically prepared test structures, and the calculated shunt currents from the method agreed well with directly measured current values. This test structure closely simulates the effect of point-like recombination-active defects after the emitter diffusion. The assumption of an ideality factor of unity that is underlying our theoretical approach is found to be reasonable even in the surrounding of local shunts.

Two methods were presented; firstly the *local $PL^0$ method* for cells and wafers that is particularly accurate and applicable for a quantitative assessment of local defects that are introduced in solar cell process steps, provided the process does not significantly alter the properties of the majority of cell area. Various specific processes that are used for local contact formation, such as laser doping, inkjet printing and plating, fall into that category.

The *global $PL^0$ method* is applicable to wafers and solar cells. Its accuracy when applied to fully metallised cells is limited by the ability to apply correction factors for currents that are supplied to the defect via the metal grid. Experimental data that show how such correction factors can be measured were presented; however, the data in this study were limited by unusually high experimental variations in the test cell contact and finger resistance.

The second source or error in the *global $PL^0$ method* is the selection of a global value for $PL^0$. This error can be minimised by selecting $PL^0$ as the average PL signal at the circumference of the analysed region. The global $PL^0$ method can also be used to quantify the recombination current in linear features such as cracks, grain boundaries and dislocations.

## ACKNOWLEDGEMENTS

Yael Augarten would like to acknowledge Robert Bardos, UNSW, for his help with the experiments and Tom Puzzer, John Durrant, Ned Western, Andrew Wrigley, Jan-Martin Wagner, Diana Thomas, Daniel Lockau and Christian Gutsche for the useful comments. The authors thank the Go8 Australia–Germany Joint Research Co-operation Scheme 2008 that resulted in the cooperation between the MPI-MSP Halle and UNSW.

## REFERENCES

1. Carstensen J, Popkirov G, Bahr J, Föll H. CELLO: an advanced LBIC measurement technique for solar cell local characterization. *Solar Energy Materials and Solar Cells* 2003; **76**(4): 599–611.
2. Van der Heide ASH, Schönecker A, Wyers GP, Sinke WC, Energy ECNS. Mapping of contact resistance and locating shunts on solar cells using resistance analysis by mapping of potential (RAMP) techniques. *Proceedings of the 16th European Photovoltaic Solar Energy Conference*, 2000; 1438–1442.
3. Donolato C. Theory of beam induced current characterization of grain boundaries in polycrystalline solar cells. *Journal of Applied Physics* 1983; **54**: 1314.
4. Marek J. Light beam induced current characterization of grain boundaries. *Journal of Applied Physics* 1984; **55**: 318.
5. Breitenstein O, Langenkamp M. *Lock-in thermography: basics and use for functional diagnostics of electronic components*. Springer Verlag, Berlin, Heidelberg, New York, 2003.
6. Kasemann M, Walter, B, Warta W. Reliable hot-spot classification in 10 ms using ultra-fast lock-in thermography. *Progress in Photovoltaics: Research and Applications* 2009; **17**: 441–450.
7. Fuyuki T, Kondo H, Yamazaki T, Takahashi Y, Uraoka Y. Photographic surveying of minority carrier diffusion length in polycrystalline silicon solar cells by electroluminescence. *Applied Physics Letters* 2005; **86**: 262108.
8. Trupke T, Bardos RA, Schubert MC, Warta W. Photoluminescence imaging of silicon wafers. *Applied Physics Letters* 2006; **89**: 044107.
9. Ballif C, Peters S, Isenberg J, Riepe S, Borchert D. Shunt imaging in solar cells using low cost commercial liquid crystal sheets. *29th IEEE Photovoltaic Specialists Conference*, New Orleans, Louisianna, 2002; 446.
10. Breitenstein O, Rakotoniaina JP, Schmidt J. Comparison of shunt imaging by liquid crystal sheets and lock-in thermography. *12th Workshop on Crystalline Silicon Solar Cell Materials and Processes*, Breckenridge, Colorado, 2002.
11. Kampwerth H, Trupke T, Weber JW, Augarten Y. Advanced luminescence based effective series resistance imaging of silicon solar cells. *Applied Physics Letters* 2008; **93**: 202102.
12. Trupke T, Pink E, Bardos RA, Abbott MD. Spatially resolved series resistance of silicon solar cells obtained from luminescence imaging. *Applied Physics Letters* 2007; **90**: 093506.
13. Glatthaar M, Giesecke J, Kasemann M, Haunschild J, Warta W, Rein S. Spatially resolved determination of the dark saturation current of silicon solar cells from electroluminescence images. *Journal of Applied Physics* 2009; **105**: 113110.
14. Giesecke JA, Kasemann M, Schubert MC, Würfel P, Warta W. Separation of local bulk and surface recombination in crystalline silicon from luminescence reabsorption.

*Progress in Photovoltaics: Research and Applications* 2009; **18**: 10–19.
15. Breitenstein O, Bauer J, Trupke T, Bardos RA. On the detection of shunts in silicon solar cells by photo-and electroluminescence imaging. *Progress in Photovoltaics* 2008; **16**: 325.
16. Trupke T, Bardos RA, Abbott MD, Fisher K, Bauer J, Breitenstein O. Luminescence imaging for fast shunt localisation in silicon solar cells and silicon wafers. *International Workshop on Science and Technology of Crystalline Silicon Solar Cells, Sendai, Japan*, 2006; 2–3.
17. Schick K, Daub E, Finkbeiner S, Würfel P. Verification of a generalized Planck law for luminescence radiation from silicon solar cells. *Applied Physics A: Materials Science and Processing* 1992; **54**: 109–114.
18. Würfel P. The chemical potential of radiation. *Journal of Physics C: Solid State Physics* 1982; **15**: 3967–3985.
19. Würfel P, Ruppel W. Chemical potential of luminescent radiation. *Journal of Luminescence* 1981; **24–25**(2): 925–928.
20. Abbott MD, Bardos RA, Trupke T, Fisher KC, Pink E. The effect of diffusion-limited lifetime on implied current voltage curves based on photoluminescence data. *Journal of Applied Physics* 2007; **102**: 044502.
21. Bauer J, Breitenstein O, Becker M, Lenzner J. Electrical investigations on SiC precipitates found in block-cast solar silicon. *Seventh NREL Workshop on Crystalline Silicon Solar Cells and Modules: Materials and Processes*, Vail, USA, 2007.
22. Kasemann M, Schubert MC, Köber M, Hermle M, Warta W. Comparison of luminescence imaging and illuminated lock-in thermography on silicon solar cells. *Applied Physics Letters* 2006; **89**: 224102.
23. Breitenstein O, Rakotoniaina JP, Rifai MHA. Quantitative evaluation of shunts in solar cells by lock-in thermography. *Progress in Photovoltaics Research and Applications* 2003; **11**: 515–526.
24. Würfel P, Trupke T, Puzzer T, Schäffer E, Warta W, Glunz SW. Diffusion lengths of silicon solar cells from luminescence images. *Journal of Applied Physics* 2007; **101**: 123110.
25. Kasemann M. Luminescence imaging for the detection of shunts on silicon solar cells. *Progress in Photovoltaics* 2008; **16**: 297–305.